Climate Dynamics
https://doi.org/10.1007/s00382-023-06972-8

What is the effect of atmospheric initial condition inconsistency between the hindcasts and real-time forecasts?

Suryun Ham[1] · Yeomin Jeong[2] · Jin Ho Yoo[1] · Somin Lim[3] · Heesook Ji[3] · Yu-Kyung Hyun[3]

Received: 2 May 2023 / Accepted: 22 September 2023

Abstract

The effects of initial errors in the subseasonal prediction are investigated using the Korea Meteorological Administration (KMA) Global Seasonal Forecasting System version 5 (GloSea5). Two experiments are designed that utilized (1) analysis data from weather prediction and (2) reanalysis data as the atmospheric initial conditions, which are considered processes of the current operational system. A comparison of these two experiments reveals the effect of the atmospheric initial conditions on subseasonal prediction. Additionally, the effects of different initial prescriptions on the hindcasts and forecasts are investigated. GloSea5 generally represents the observed temperature patterns well; however, cold biases are distinct over continents in the Northern Hemisphere, including the East Asia region in the hindcast results. However, the forecast results simulate anomalously high temperatures in most regions, except for parts of the polar and Australian regions. In this study, it is clear that improved atmospheric initial conditions lead to changes in the prediction skills of variables related to seasonal climate variability in mid-latitude regions. In addition, the biases of the surface temperature are reduced in most regions when the atmospheric initial condition are made consistent between the hindcast and forecast. Notably, increased initial errors in real-time forecasts, compared to hindcasts, can cause more biases in surface temperature and atmospheric circulation fields on a subseasonal time scale.

Keywords Initial condition · Subseasonal prediction · KMA GloSea5

1 Introduction

Climate prediction models are continuously being developed to improve mid- to long-term prediction skill within the global operational prediction community. Since 1999, the Korea Meteorological Administration (KMA) has conducted a long-term forecast system using a global prediction system based on dynamical processes. In 2010, to improve seasonal prediction skills, fully-coupled atmosphere, land, ocean, and sea-ice model was established based on the Global Seasonal Forecasting System (GloSea4) of United Kingdom Meteorological Office (UKMO). Recently, GloSea6, after GloSea4 and Glosea5, with improved physical processes and high horizontal resolution, has been used in operational prediction models (MacLachlan et al. 2015).

Many operational institutions and research centers worldwide have been developing prediction systems that can make seamless forecasts for long-term climate, as well as short-term weather to seasonal climate. Subseasonal to seasonal (S2S) prediction bridges the gap between weather and seasonal climate forecasts (Vitart et al. 2019). The S2S time scale has not received much attention in the past, however, its importance has grown with the recent demand for predicting extreme weather and climate events. Accordingly, the launch of various S2S prediction projects has been made in better understanding potential sources of S2S prediction and improve prediction skills (Viart et al. 2017). Many studies have reported on seasonal predictability that are strongly related to tropical rainfall prediction and its teleconnection to extratropical circulation such as El Niño–Southern Oscillation, Arctic Oscillation, and Pacific North American patterns (Kumar et al. 2013; Scaife et al. 2019; Li et al. 2016). Recently, it is also well known that the subseasonal

✉ Suryun Ham
suryun01@gmail.com

[1] Climate Services and Research Division, APEC Climate Center, Busan, Korea

[2] Institute of Environmental Studies, Pusan National University, Busan, Korea

[3] Climate Research Department, National Institute of Meteorological Sciences, Seogwipo, Korea

predictability is expressed by simulating various phenomena in the atmosphere, ocean, sea-ice, and land (such as Madden–Julian oscillation, El Nino-Southern Oscillation, Arctic Oscillation, tropical convection, tropical cyclones, sea-ice cover, soil moisture, snow cover, stratosphere condition, ocean status, and various teleconnections), although there are still room for further understanding (Lim et al. 2018; Zampieri et al. 2018; Choi and Son 2019; Nie et al. 2019; Lang et al. 2020; Mariotti et al. 2020; Merryfield et al. 2020; Oh et al. 2022).

Notable, initial atmospheric conditions can substantially affect weather forecasting. The influence of initial atmospheric conditions that are considered important on short-time scales, such as surface and atmospheric processes, has been receiving increasing attention. In particular, initial condition studies for seamless climate prediction systems including their sources of predictability from seasonal to subseasonal scale, are growing in number. Numerous studies have suggested that potential predictability can be improved by initial land conditions and land surface processes in the prediction models (Koster et al. 2010; Guo et al. 2011; Materia et al. 2014). In addition, many studies have revealed that realistic initialization of soil moisture substantially improves the simulation of surface air temperature prediction skills through land–atmosphere feedback (Miralles et al. 2014; Hauser et al. 2016; Orth et al. 2016; Seo et al. 2019).

Although initial atmospheric conditions have received less attention in seasonal climate prediction, some studies have revealed that the initial atmospheric state can affect seasonal forecasts (Stockdale et al. 2015; Marshall and Scaife 2010; Rao et al. 2023). In addition, some studies have suggested that initial atmospheric conditions can impact subseasonal forecasts (Lin et al. 2010; Vitart et al. 2019). For example, Lin et al. suggested that the skill of the North Atlantic Oscillation (NAO) forecast could be improved according to the Madden–Julian Oscillation (MJO) strength and phase in the initial condition. Vitart et al. (2019) mentioned that initializing experiments with different atmospheric reanalysis data largely improved the extended-range skill scores up to week four. These results indicated that the initial state and data played important roles in assessing the reliability of forecasts and reducing forecast uncertainty.

Despite many efforts to improve the initial conditions, there is another limitation pertaining the production of the initial conditions under operational climate prediction model. In operational institutions and research centers around the world, the initial conditions of hindcasts and forecasts are often given differently due to the time constraints for real-time forecasting. For example, the KMA subseasonal and seasonal prediction system uses reanalysis data as the atmospheric initial condition for the hindcast but uses analysis data from the weather prediction model with data assimilation for real-time forecasting. This inconsistency in the initial conditions of the real-time forecasts can directly affect the anomaly fields produced when the hindcast climatology is subtracted from the forecast. However, the difference between the initial conditions of the hindcast and forecast has been disregarded in many operational centers.

In this study, we investigated how the consistency between atmospheric initial conditions in hindcasts and real-time forecasts affects subseasonal prediction skill. In particular, the analysis was based on an operational subseasonal prediction system in the KMA. This study is divided into the following sections: a brief description of the KMA operational model and a sensitive experimental design is provided in Sect. 2; Sect. 3 investigates the effect of the initial atmospheric condition on subseasonal prediction; and Sect. 4 summarizes the results and provides major conclusions.

2 Model and data description

In this study, a subseasonal dataset produced by the operational KMA prediction system was used. The KMA has an operational subseasonal to seasonal forecast system, which is a joint system between the KMA and the UK Met Office. The Global Seasonal Forecasting System version 4, and 5 (hereafter, GloSea4, and GloSea5, respectively), are the operational subseasonal forecast system of the KMA. This system was upgraded to version6 (hereafter GloSea6). However, in this study, GloSea5 was used to investigated the effects of inconsistency between the initial conditions of hindcasts and forecasts on a subseasonal time scale.

GloSea5 is a fully coupled global climate model that consists of atmosphere (Unified Model; UM), ocean (Nucleus for European Modeling of the Ocean; NEMO), land surface (Joint UK Land Environment Simulator; JULES), and sea ice (Los Alamos sea ice model; CICE) components through the coupler OASIS (MacLachlan et al. 2015). The resolution is N216N85 (approximately 60 km) for the atmosphere, and ORCA0.25L75 (0.25° on a tri-polar grid) for the ocean. A Stochastic Kinetic Energy Backscatter scheme (SKEB) is used to generate the spread between members initialized from the same analysis. Further detailed information on GloSea5 is provided by MacLachlan et al. (2015).

To investigate the effect of initial atmospheric conditions on subseasonal prediction skill, two forecast experiments are designed namely NWPiF and ERAiF. Due to time limitations in real-time forecasting, the analyzed data is used for data assimilation with limited observational data. The NWPiF experiment has the same setting as the current operational real-time forecast, which uses the analysis data from the UM Global Data Assimilation and Prediction System (GDAPS) as the initial atmospheric conditions. The ERAiF experiment uses ERA-interim reanalysis data (ERA-interim; Dee et al. 2011) instead of analysis data as the initial atmospheric conditions same as the hindcast setup. This experiment is only an initial condition that is different from NWPiF. A comparison of these two experiments revealed the effect of the initial atmospheric conditions on subseasonal prediction. In addition, the effects of different initial condition prescriptions on the hindcast and forecast are investigated.

Two experiments are conducted with more than 200 members covering the forecasting period from November 2017 to December 2018. Each case (one initialized run) consists of four ensemble members using the SKEB method, which are initialized on fixed calendar dates: the 1st, 9th, 17th, and 25th of each month. All cases from the initialized start dates with four ensemble members are integrated over a 60-day period for subseasonal to seasonal predictions. The DJF 2017–2018 forecast period in relation to the initial error, NDJFMA 2017–2018 forecast period in relation to equatorial variability, and JJA 2018 forecast period for the East Asian summer monsoon are analyzed. In addition, the results from all cases for 2018 are utilized to validate the subseasonal prediction skill score.

For validation of various features related to the initial condition in GloSea5, ECMWF reanalysis version5 (ERA5; Hersbach et al. 2018) and the Global Precipitation Climatology Project (GPCP) version 2.1 combined precipitation dataset (Adler et al. 2003) are used in this study.

3 Results

Figure 1 shows the spatial distribution of the surface temperature biases of 3–4 weeks lead from to the 1991–2010 hindcast period and the 2017–2018 real-time forecast period. The hindcast results generally show an error of less than 2° on land. Except for some parts of the equational areas, it is characterized by cold biases globally. In addition, there are warm biases along some equatorial regions in South America, Africa, and the Maritime Continental Area. However, the forecast results simulate anomalously high temperatures in most regions, except for parts of the polar and Australian regions.

Although the hindcast has good prediction skill, many operational institutions suffer from uncertainty in real-time forecasts. The occurrence of errors in the hindcast and forecast at different could be attributed to the fact that if the error of the real-time forecast and hindcast has a different pattern, then the anomaly can have a greater error, even though anomaly with removal of the hindcast climatology in real-time forecasts is widely used as a method to remove systematic error. Nevertheless, the method of anomaly removing the hindcast climatology may be the best way to eliminate systematic errors. To overcome this limitation, there is a method for obtaining an anomaly by correcting errors in hindcast climatology. Among the various reasons for such conflicting biases between the hindcast and forecast in Fig. 1, the biggest possible reason could be the excessive cold biases of the hindcast. In this study, the method of bias correction is not considered, and the effects of different prescriptions of the initial data of the hindcast and forecast is investigated.

3.1 Initial error distribution

To examine how the initial condition difference affected atmospheric phenomena, the difference distribution of some variables at the 1–day lead from each experiment for DJF 2017–2018 is compared with the reanalysis data because winter temperature errors are shown clearly. Because the values of 00UTC is used as the atmospheric initial condition of the two experiments, the comparison of the initial error used the daily average value for 1 day of integration, and expressed it as a 1–day lead time. In addition, since the 1–day integral values are compared, the difference between the two initial conditions excluding the initial systematic error can be investigated.

Figure 2 shows the difference in the distribution of the top (0–0.1m) soil temperature below the surface and ice concentration from two experiments with a 1-day lead time. The

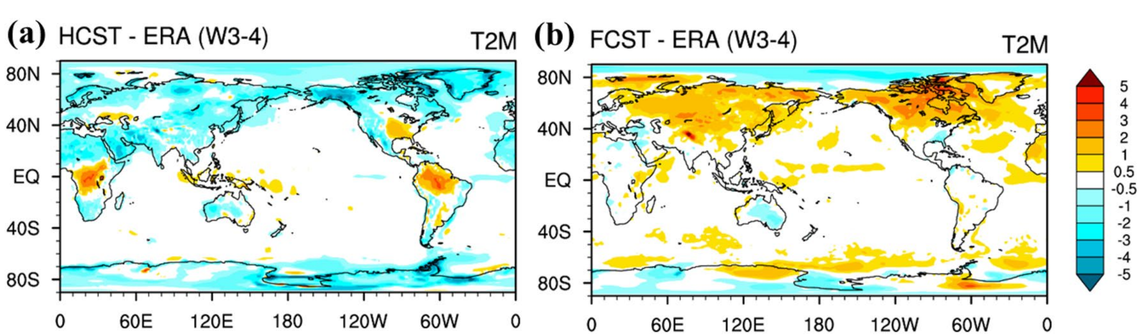

Fig. 1 Spatial distribution of surface temperature (K) biases (model minus ERA5 reanalysis) of 3–4 weeks lead from **a** hindcast periods and **b** 2017–2018 forecast periods

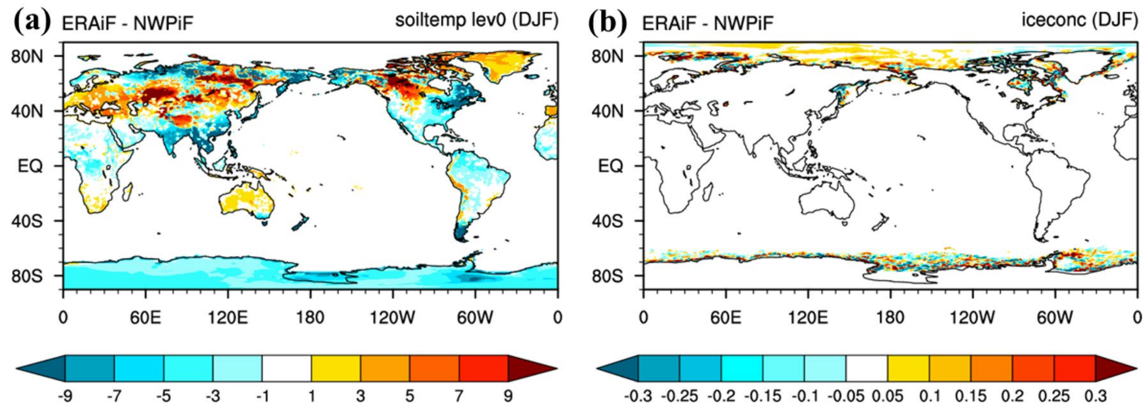

Fig. 2 Difference distribution of **a** surface soil temperature (K) and **b** ice concentration for 2017–2018 DJF at 1–day lead between ERAiF and NWPiF

ERAiF experiment shows a higher soil temperature than the NWPiF experiment in the highland area around a latitude of 40°N, but a low temperature shown in most areas. In the ice concentration results, there is a noise difference in the Antarctic. However, in the Arctic, the experiment using the reanalysis data as the initial field shows a higher concentration than the experiment using the analysis data from the NWP model as the initial field.

The variables of the cloud-radiation-precipitation processes related to surface temperature also show a large difference between the two experiments (Fig. 3). The ERAiF experiment simulates less precipitation than the NWPiF experiment at 1– day lead time (Fig. 3a). The difference in precipitation between the two experiments could be attributed to the cloud simulation results. When the reanalysis data is used as the initial conditions, the number of clouds decreases compared to when the analysis data from the NWP model is used as the initial field (Fig. 3b). Reduced clouds increase surface shortwave radiation and outgoing longwave radiation because they pass through them without reflection (Fig. 3c, d). The reason for the cloud difference between the NWPiF and ERAiF experiments will be

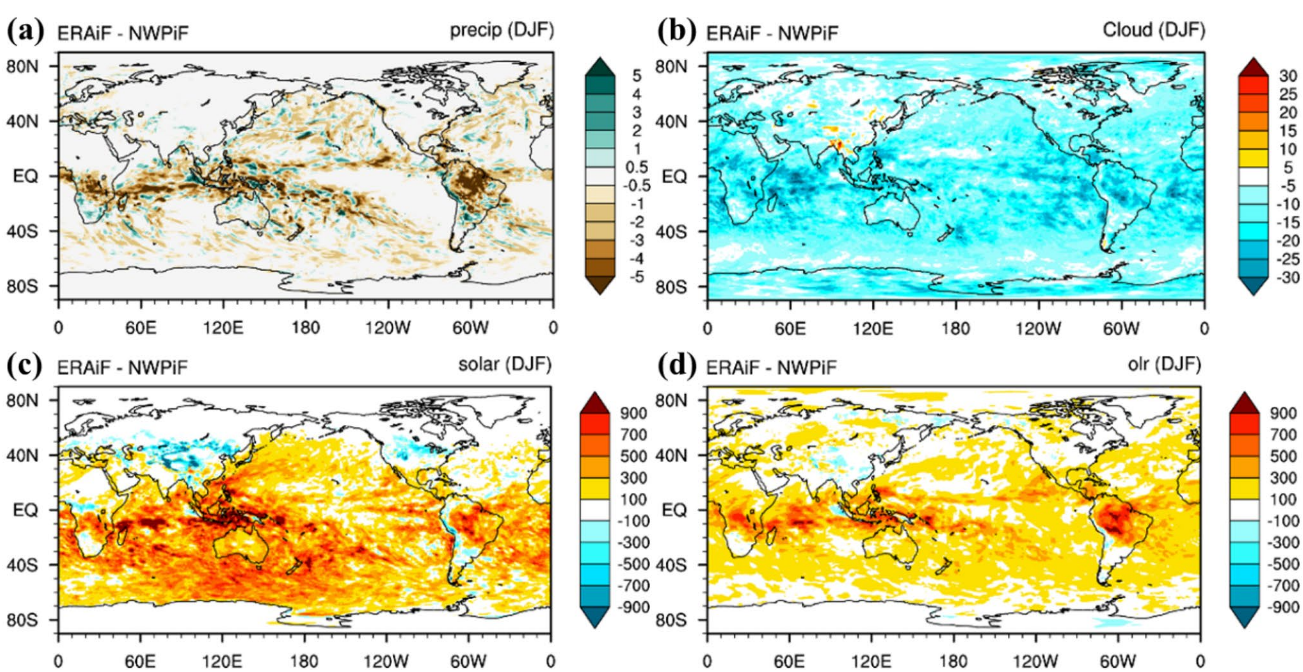

Fig. 3 Difference distribution of **a** surface precipitation (mm/day), **b** total cloud amount (%), **c** solar radiation fluxes (W/m^2), and outgoing long-wave radiation fluxes (W/m^2) for 2017–2018 DJF at 1–day lead between ERAiF and NWPiF

examined separately; in this study, only the effect of the difference between the two datasets on subseasonal prediction is examined.

3.2 Predictability of tropical variability

To examine how differences in the initial field affect subseasonal forecasting, the simulation results of tropical variability, which is the most representative phenomenon in intraseasonal prediction, are compared. The precipitation biases of 3–4 lead weeks from NWPiF, which is the default setting for the operational prediction system, are shown in Fig. 4a. The NWPiF experiment exhibits wet biases from the Indian Ocean to the western Pacific and dry biases in the central Pacific. Although the difference in precipitation between the ERAiF and NWPiF experiments are not significant, it slightly reduces the biases in the ERAiF experiment (Fig. 4b).

There is no large changes with a slight improvement in the mean precipitation of the 3– 4 lead weeks by the initial condition, but the MJO prediction, which is a representative phenomenon of subseasonal variability, is quite different. Figure 5 shows the bivariate correlation coefficients for the velocity potential MJO indices in the two experiments and their hindcasts. The lead time when the hindcast reaches a correlation coefficient of 0.5 (an indicator of useful skill) is approximately 19–day (Fig 5a, black line). General MJO index (ex. RMM) using the GloSea5 OLR is known to be 25–27 days longer than the index using the velocity potential (Kim et al. 2019). In the period when the experiments were conducted, the lead time for the bivariate correlation coefficients to reach 0.5 is approximately 4–5 days longer than the hindcast results. In particular, the ERAiF experiment using the reanalysis data as the initial condition shows a slower rate of decrease in the MJO index as the lead time increased, compared with the NWPiF experiment. The 1–2 lead weeks averaged MJO index between the two experiments is similar, but the 3–4 lead weeks averaged index shows a difference of approximately 0.1.

To examine the MJO propagation characteristics, the results from the extended winter period (November 2017 to April 2018) are shown in Figs. 6, 7, and 8. The zonal wind at

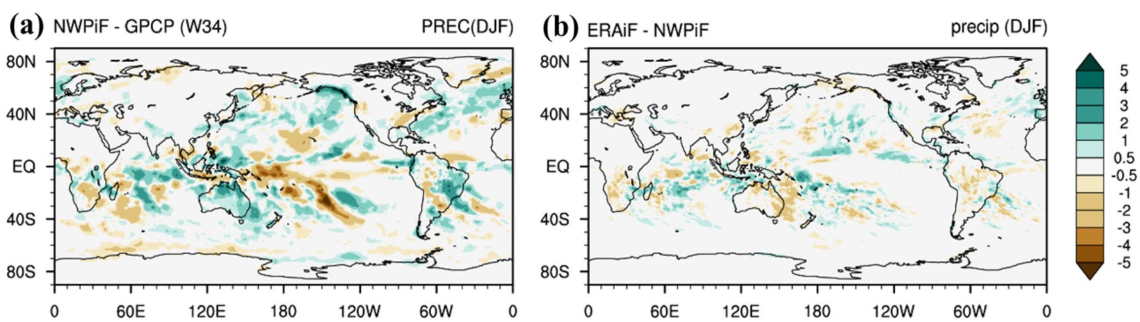

Fig. 4 Difference distribution of surface precipitation (mm/day) for 2017–2018 DJF at lead weeks 3–4 between **a** NWPiF and ERA5 and **b** ERAiF and NWPiF

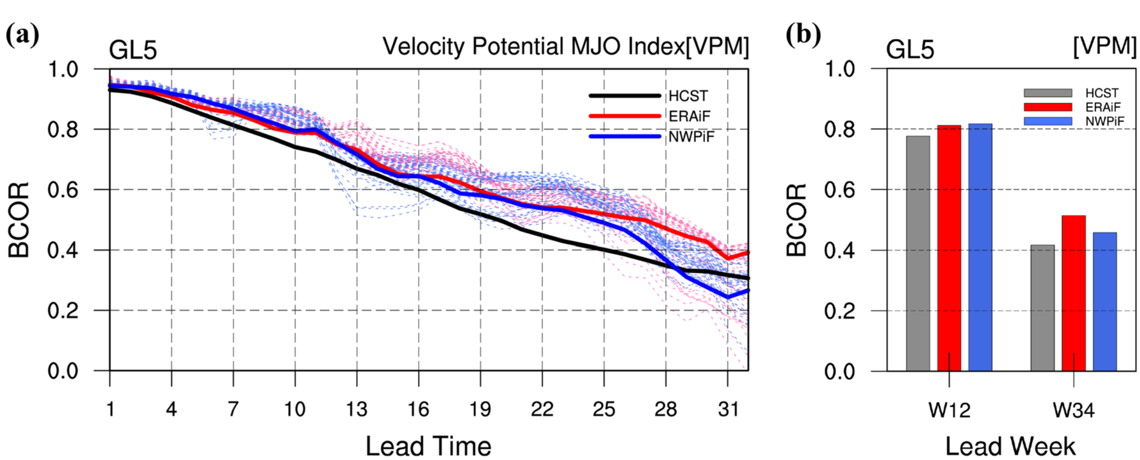

Fig. 5 **a** Daily and **b** weekly bivariate Correlation coefficient (BCOR) for velocity potential Madden–Julian Oscillation (MJO) indices in GloSea5 hindcast (black, grey), ERAiF (red), and NWPiF (blue) experiments. Dotted lines indicate each case runs with different initial conditions

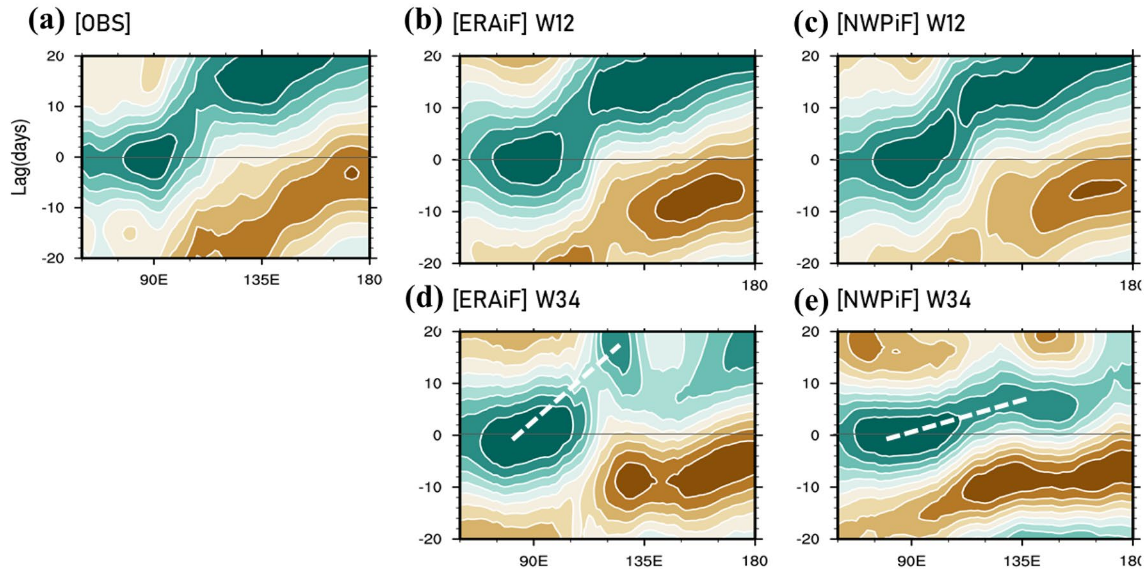

Fig. 6 Lag time-longitude correlation (i.e. Madden–Julian Oscillation (MJO) propagation diagram) of 850 hPa zonal wind in ERA5 reanalysis data (OBS) and ERAiF experiment, and NWPiF experiment during the extended winter (Dec 2017–Apr 2018) (60–180E, 10S–10N, 20–70 days filtered)

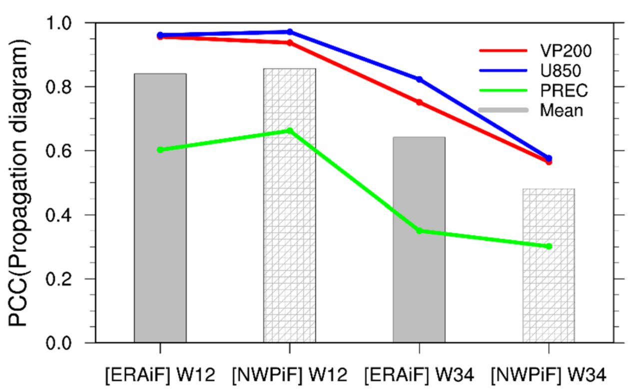

Fig. 7 Pattern correlation coefficient skill of Madden–Julian Oscillation (MJO) propagation diagram (60–180E, 10S–10N, 20–70 days filtered) for 850 hPa zonal wind (U850), 200 hPa vorticity potential (VP200), precipitation (PREC), and the mean of all variables during the extended winter (Dec 2017–Apr 2018) from ERAiF (filled bar) and NWPiF (patterned bar) experiments

850 hPa anomalies are averaged over 10°S-10°N and is displayed as a function of longitude and forecast lead (Fig. 6). Both experiments on 1–2 lead weeks are shown a relatively well-organized eastward propagation with low-level easterly winds preceding convection. The predicted low-level wind anomaly for 1–2 weeks lead shows eastward propagation to the eastern Pacific over day 20, which is exhibited in the reanalysis. However, the results of the 3–4 weeks lead from the two experiments predict quite differ from the observed pattern. The NWPiF experiment shows that the eastward propagation speed of the low-level wind anomaly is fast and even reverses the phase in the eastern Pacific at lag day 10. Although the ERAiF experiment also shows that the anomalies of low-level winds in the eastern Pacific break slightly around lag day 10, it predicts a pattern that is more similar to that observed in the NWPiF experiment.

The MJO propagation diagram of the upper vorticity potential (VP200), low-level zonal wind (U850), precipitation (PREC), and the mean of all variables from each experiment is compared with the observations, and as shown in Fig. 7, as the pattern correlation coefficients. For lead 1–2 weeks, the two experiments have similar correlation coefficients with high values > 0.5 and > 0.9, for precipitation and large-scale variables, respectively. At lead 3–4 weeks, the propagation skills are lower than at lead 1–2 weeks. In particular, the NWPiF experiment exhibits a lower correlation coefficient than the ERAiF experiment. Interestingly, while the precipitation skills of the two experiments are similar, the ERAiF experiment shows a much higher correlation coefficient than the NWPiF experiment for large-scale circulation variables. In other words, it is noted that the difference in atmospheric initial condition can affect large-scale circulation in lead 3–4 weeks, which can further improve MJO prediction skills.

3.3 Subseasonal prediction skill over East Asia

It is clear that the initial data can affect equatorial variability prediction skills, but how does it affects the mid-latitude? The East Asian summer monsoon (EASM) is a representative phenomenon that has a significant influence

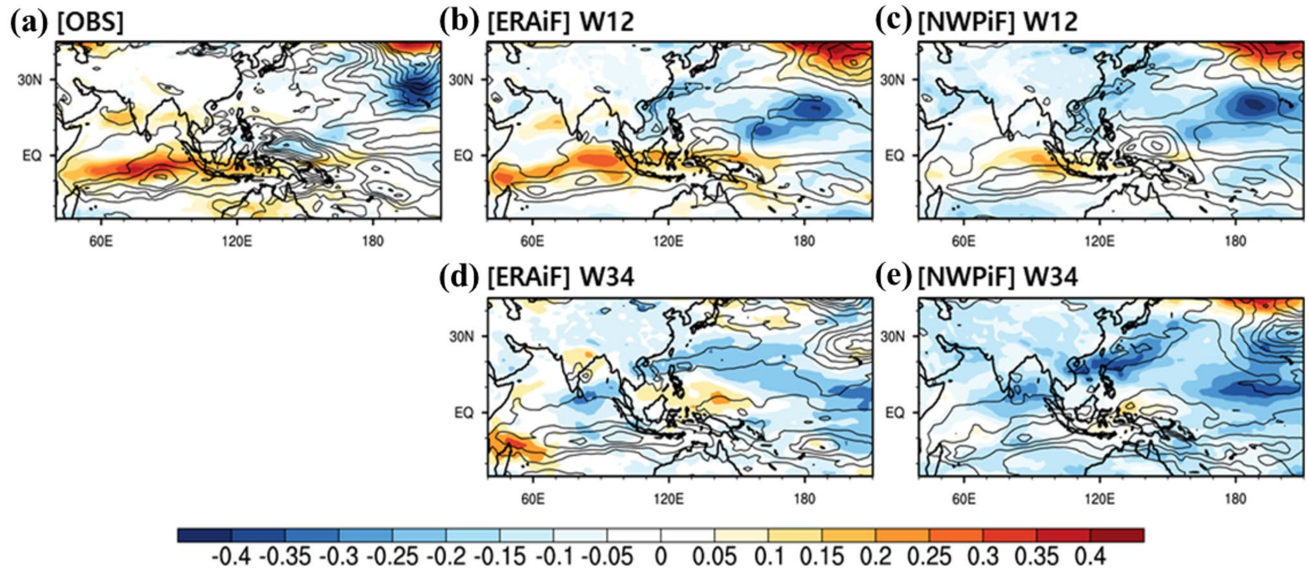

Fig. 8 Spatial distributions of mean (shading) and variance (contour) fields for 850 hPa zonal wind (m/s) for 2018 JJA in **a** observation, **b** and **d** ERAiF, and **c** and **e** NWPiF experiments, respectively

on temperature and precipitation in the Korean Peninsula. Changes in large-scale circulations in MJO and EASM predictions in low-latitude regions can affect the subseasonal prediction skill in mid-latitudes through teleconnection. Therefore, this study examines the results for the forecast period JJA, 2018, to investigate the effects of differences in initial conditions on EASM features over mid-latitude regions.

Overall, the 850 hPa zonal wind plays an important role in modulating the strength and direction of the EASM. Figure 8 shows the spatial distributions of the averaged anomalies and variance fields for 850 hPa zonal winds in the observations and two experiments. The observed zonal wind distribution shows a positive anomaly from the Indian Ocean to the Maritime Continent and a negative anomaly in the Northwest Pacific. Furthermore, it also shows the strongest variance between the Indian Ocean and the Northwest Pacific. In both experiments, the results of lead for 1–2 weeks generally simulate the characteristics of the observations well, with some biases. For the ERAiF experiment, the simulated variance is similar to the observed pattern, while the mean field weakly simulates a positive anomaly in the Indian Ocean region. Weak negative anomalies are noticeable in the western Pacific. For the NWPiF experiment, the negative anomaly in the Indian Ocean becomes weaker and the negative anomaly in the western Pacific becomes stronger compared with the ERAiF experiment. The results of lead 3–4 weeks, the ERAiF experiment appears closer to the observation than the NWPiF experiment. In particular, the NWPiF experiment shows that the wind field significantly decreased in most areas from the Indian Ocean to the western Pacific.

When the 850 hPa zonal wind is weak, it can strengthen the EASM by allowing more moisture to be transported to the region. Weak zonal winds can lead to a more meridional monsoon flow, which can enhance the transport of moisture from the tropics to the mid-latitudes. Figure 9a shows the difference in the distribution of 850 hPa wind fields between the ERAiF and NWPiF experiments. Compared with the NWPiF experiment, the ERAiF experiment shows strong easterly winds at low–latitudes, which leads to enhanced southerly winds at mid-latitudes. The ERAiF experiment strengthens the updraft in the western Pacific and weakens the downdraft at mid-latitudes owing to secondary circulation (Fig. 9b). As a result, the specific humidity near the surface in the mid-latitudes increased in the ERAiF experiment compared to that in the NWPiF experiment.

Figure 10 shows the spatial distribution of the precipitation biases in the NWPiF experiment and the differences between the two experiments. GPCP observations show that the summer precipitation pattern peaks over the intertropical convergence zone in the Pacific and regions from the western Pacific to the South China Sea, which is representative of EASM patterns (not shown here). The NWPiF experiments generally well captures the observed wet regions. However there are dry biases from the Maritime Continent to the western Pacific, including the South China Sea. The ERAiF experiment effectively reduces biases by increasing precipitation in the western Pacific. In addition, precipitation

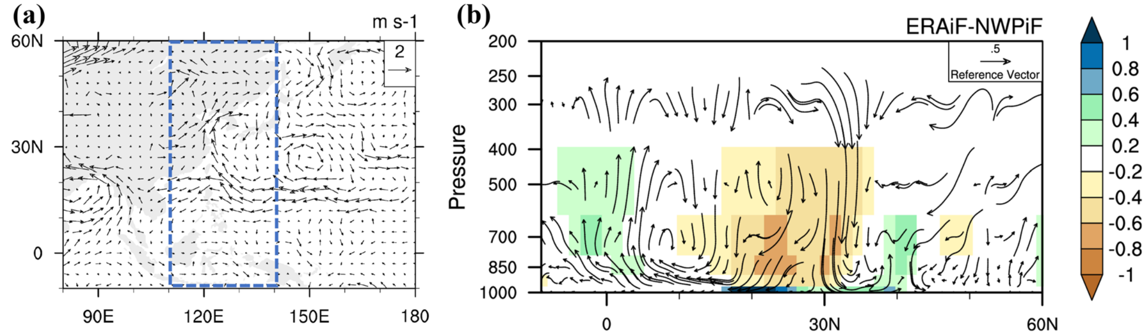

Fig. 9 Difference distributions of **a** 850 hPa wind (m/s), and **b** averaged (blue box; 110E–140E) meridional mean specific humidity (kg/kg) (shading), meridional and vertical circulation (arrows) for 2018 JJA between ERAiF and NWPiF experiments

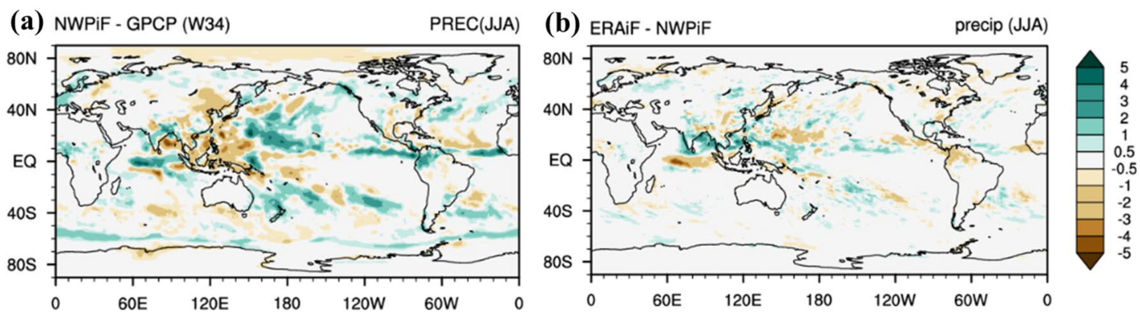

Fig. 10 Difference distribution of surface precipitation (mm/day) for 2018 JJA at lead weeks 3–4 between **a** NWPiF and ERA5 and, **b** ERAiF and NWPiF

in the Indian Ocean and equatorial Pacific is similar to that observed in the ERAiF experiment.

Finally, it is examined how the featured biases in the forecast affect the prediction skills by the initial condition. The NWPiF experiment shows prominent warm biases for JJA over globe, as shown in Fig. 1b (not shown here). Notably, the temperature biases exhibits the same pattern as the positive signs in both summer and winter. Clearly, warm biases are characteristic of systematic errors in GloSea5. Compared with the NWPiF experiment, the ERAiF experiment simulates lower surface temperatures in East Asia and parts of America (Fig. 11a). To examine the degree of improvement caused by the initial conditions, the rate of change of the root mean square error (RMSE) of the two experiments is plotted in Fig. 11b. It is clear that the RMSE decrease in most regions owing to changes in the initial conditions using reanalysis data. In particular, there are remarkable improvements in areas such as East Asia, where warm biases have decreased.

Figure 12 shows the anomaly correlation coefficient of surface temperature and 500 hPa geopotential height from two experiments over globe and East Asia according to lead weeks 1–8. In both experiments, prediction skills gradually decrease according to the lead week. Although the prediction performance of the two experiments has not much difference, it is clear that a more accurate initial condition leads to a higher correlation coefficient even with a subseasonal time period such as 3–4 lead weeks.

4 Concluding remarks

The effects of the initial condition errors on the subseasonal prediction is investigated using the KMA GloSea5. GloSea5 generally represents the observed temperature patterns well; however, cold biases are distinct over continents in the Northern Hemisphere, including the East Asia region in the hindcast results. However, the forecast results simulate anomalously high temperatures in most regions, except for parts of the polar and Australian regions. Among the reasons for such conflicting biases between hindcasts and forecasts, the biggest possible reason may be excessive cold biases of the hindcast. In this study, the method of bias correction is not considered, and the effects of the different prescriptions of the initial data of the hindcast and forecast is investigated.

Two experiments are designed: NWPiF and ERAiF. The ERAiF experiment uses the analysis data of the UM GDAPS as the initial atmospheric conditions, which has the same

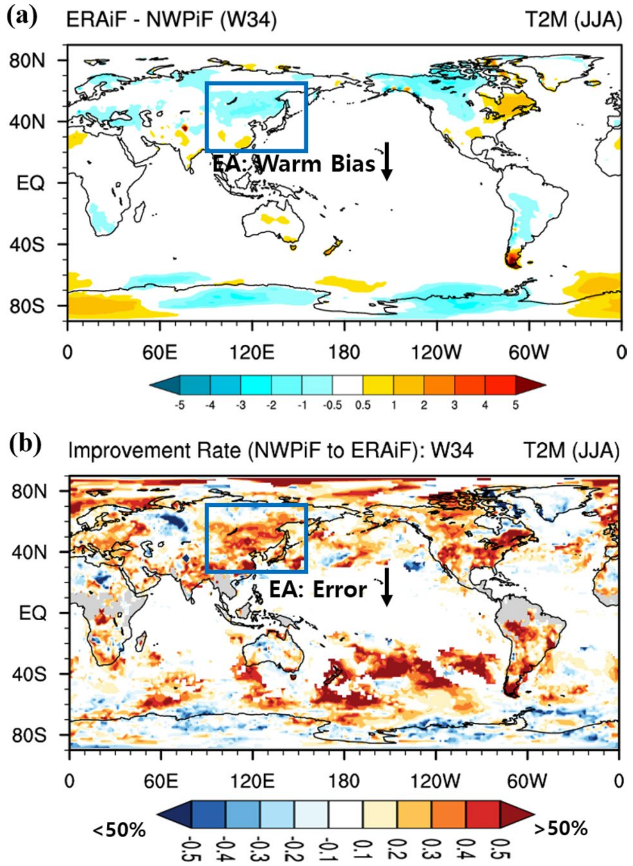

Fig. 11 **a** Difference distribution of surface temperature (K) at lead weeks 3–4 between ERAiF and NWPiF. **b** Improvement rate (%) (the rate of change of RMSE of the two experiments) of the ERAiF compare to the NWPiF using RMSE of surface temperature at lead weeks 3–4

settings as an operational real-time forecast. The ERAiF experiment uses ERA-interim reanalysis data as the initial atmospheric conditions, same as the hindcast setup. This experiment is only an initial condition that is different from NWPiF. A comparison of these two experiments reveals the effect of the initial atmospheric conditions on the subseasonal prediction. In addition, the effects of different initial condition prescriptions of hindcasts and forecasts are investigated on a subseasonal time scale.

MJO prediction, such as bivariate correlation coefficients, is clearly improved by the initial atmospheric conditions. The NWPiF experiment on 3–4 lead weeks shows that the eastward propagation speed of the low-level wind anomaly is rapid and even reverses its phase in the eastern Pacific. However, the ERAiF experiment predicts a pattern similar to that observed in the NWPiF experiment. The improved initial atmospheric conditions leads to changes in the prediction skills of variables related to seasonal climate variability in the mid-latitude regions. The variance fields for 850 hPa zonal winds from the ERAiF experiment show significantly improvment in most areas from the Indian Ocean to the western Pacific compared with those from the NWPiF experiment. In addition, the ERAiF experiment effectively reduces biases by increasing precipitation in the western Pacific compared with the NWPiF experiment. In addition, the biases of the surface temperature decreased in most regions owing to the changes in the initial conditions using reanalysis data. In particular, there are remarkable improvements in warm biases such as in East Asia. In other words, the increased initial errors in the real-time forecast compared to the hindcast causes more biases in the surface temperature and atmospheric circulation fields at subseasonal time scale.

It is well known that initial condition can greatly affect the weather forecasting skill. Recently, initial condition studies for seamless climate prediction systems including their

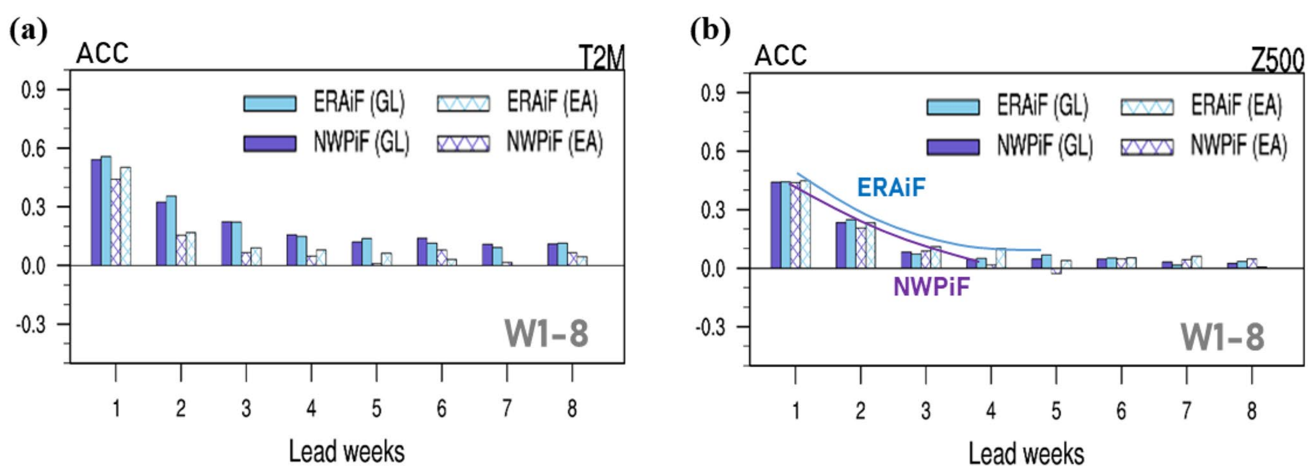

Fig. 12 Anomaly correlation coefficient of **a** surface temperature and **b** 500 hPa geopotential height from ERAiF (blue) and NWPiF (purple) experiments over globe (shaded bar) and East Asia (dashed bar)

sources of predictability from seasonal to subseasonal scales, have been growing in number. However, many operational institutions still suffer from uncertainty in real-time forecasts even though hindcasts have good prediction skills. Among the reasons for such conflicting biases between hindcasts and forecasts is the prescription of different atmospheric initial conditions due to time limitations for real-time prediction. In this study, it is revealed that the inconsistency of the initial conditions for hindcast and real-time forecasts leads to subseasonal prediction skills; in particular, tropical oscillations and mid-latitude dynamics could be affected by low-level wind fields. In conclusion, to improve the performance of real-time forecasts, it is necessary to use a more accurate initial condition such as reanalysis data used for hindcast or to prescribe an appropriate climatology to reduce the error produced from inconsistency.

Acknowledgements This research was supported by the APEC Climate Center. Experiments in this studies were conducted using a supercomputer provided by the National Center for Meteorological Supercomputer at KMA. Authors from KMA were funded by the Korea Meteorological Administration Research and Development Program "Operating and Developing Global Seasonal Forecast System (KMA2018-00320)". Author from Pusan National University was supported by Basic Science Research Program through the National Research Foundation of Korea (NRF) funded by the Ministry of Education (2020R1A6A1A03044834).

Author contributions All authors contributed to the conception and design of this study. Material preparation, data collection, and analyses were performed by SH, YJ, JHY, SL, HJ, and Y-KH. The first draft of the manuscript was written by Suryun Ham and all authors commented on previous versions of the manuscript. All the authors have read and approved the final version of the manuscript.

Funding The authors have not disclosed any funding.

Data availability The datasets analyzed during the current study are not publicly available because of network issues but are available from the corresponding author upon reasonable request.

Declarations

Conflict of interests The authors have no relevant financial or non-financial interests to disclose.

References

Adler RF et al (2003) The Version 2 Global Precipitation Clilmatology Project (GPCP) monthly precipitation analysis (1979-Present). J Hydrometeo 4:1147–1167

Choi J, Son S-W (2019) Stratospheric initial condition for skillful surface precipitation in the ECMWF model. Geophys Res Lett 46:12556–12564. https://doi.org/10.1029/2019GL083519

Dee DP et al (2011) The ERA-Interim reanalysis: configuration and performance of the data assimilation system. Quart J Roy Meteor Soc 137(656):553–597. https://doi.org/10.1002/qj.828

Guo Z, Dirmeyer PA, DelSole T (2011) Land surface impacts on subseasonal and seasonal predictability. Geophys Res Lett. https://doi.org/10.1029/2011GL049945

Hersbach H et al (2018) ERA5 hourly data on single levels from 1959 to present. Copernicus Climate Change Service (C3S) Climate Data Sore (CDS)

Kim H, Matthew AJ, Pegion K (2019) MJO propagation processes and mean biases in the SubX and S2S reforecasts. J Geophys Res Atmos 124(16):9314–9331

Koster RD et al (2010) Contribution of land surface initialization to subseasonal forecast skill: first results from a multi-model experiment. Geophys Res Lett 37:L02402. https://doi.org/10.1029/2009GL041677

Kumar A, Chen M, Wang W (2013) Understanding prediction skill of seasonal mean precipitation over the Tropics. J Climate 26:5674–5681

Lang AL, Pegion K, Barnes EA (2020) Introduction to special collection: "Bridging weather and climate: Subseasonal-to-seasonal (S2S) prediction." J Geophys Res Atmos. https://doi.org/10.1029/2019JD031833

Li C, Scaife AA, Lu R, Arribas A, Brookshaw A, Comer RE, Li J, MacLachlan C, Wu P (2016) Skillful seasonal prediction of Yangtze river valley summer rainfall. Environ Res Lett 11:094002. https://doi.org/10.1088/1748-9326/11/9/094002

Lim Y, Son S, Kim D (2018) MJO Prediction skill of the subseasonal-to-seasonal prediction models. J Climate 31:4075–4094. https://doi.org/10.1175/JCLI-D-17-0545.1

Lin H, Brunet G, Fontecilla JS (2010) Impact of the Madden-Julian Oscillation on the intraseasonal forecast skill of the North Atlantic Oscillation. Geophys Res Lett 37:L19803. https://doi.org/10.1029/2010GL044315

MacLachlan C et al (2015) Global Seasonal forecast system version 5 (GloSea5): a high-resolution seasonal forecast system. Quart J Roy Meteor Soc 141:1072–1084. https://doi.org/10.1002/qj.2396

Mariotti A et al (2020) Windows of opportunity for skillful forecasts subseasonal to seasonal and beyond. Bull Amer Meteor Soc. https://doi.org/10.1175/BAMS-D-18-0326.1

Marshall AG, Scaife AA (2010) Improved predictability of stratospheric sudden warming events in an atmospheric general circulation model with enhanced stratospheric resolution. J Geophys Res 115:D16114. https://doi.org/10.1029/2009JD012643

Materia S, Borrelli A, Bellucci A, Alessandri A, Pietro PD, Athanasiadis P, Navarra A, Gualdi S (2014) Impact of atmosphere and land surface initial conditions on seasonal forecasts of global surface temperature. J Climate 27(24):9253–9271

Merryfield WJ et al (2020) Current and emerging developments in subseasonal to decadal prediction. Bull Amer Meteor Soc 101(6):E869–E896. https://doi.org/10.1175/BAMS-D-19-0037.1

Miralles DG, Teuling AJ, van Heerwaarden CC, de Arellano JV-G (2014) Mega-heatwave temperatures due to combined soil desiccation and atmospheric heat accumulation. Nat Geosci 7(5):345

Nie Y, Scaife AA, Ren H-L, Comer RE, Andrews MB, Davis P, Martin N (2019) Stratospheric initial conditions provide seasonal predictability of the North Atlantic and Arctic Oscillations. Environ Res Lett 14:034006

Oh J, Son S-W et al (2022) Impact of stratospheric ozone on the subseasonal prediction in the southern hemisphere spring. Prog Earth Planet Sci. https://doi.org/10.1186/s40645-022-00485-4

Orth R, Dutra E, Pappenberger F (2016) Improving weather predictability by including land surface model parameter uncertainty. Mon Wea Rev 144(4):1551–1569

Rao J, Wu T, Garfinkel CI, Luo J, Lu Y, Chu M, Hu J (2023) Impact of the initial stratospheric polar vortex state on East Asian spring rainfall prediction in seasonal forecast models. Clim Dyn 60:4111–4131. https://doi.org/10.1007/s00382-022006551-3

Scaife AA, Ferranti L, Alves O et al (2019) Tropical rainfall predictions from multiple seasonal forecast systems. Int J Climatol 39:974–988. https://doi.org/10.1002/joc.5855

Seo E, Lee M-I, Jeong J-H, Koster RD, Schubert SD, Kim H-M, Kim D, Kang H-S, Kim H-K, MacLachlan C, Scaife AA (2019) Impact of soil moisture initialization on boreal summer subseasonal forecasts: mid-latitude surface air temperature and heat wave events. Clim Dyn 52:1695–1709

Stockdale TN, Molteni F, Ferranti L (2015) Atmospheric initial conditions and the predictability of the Arctic Oscillation. Geophys Res Lett 42:1173–1179

Vitart F et al (2017) The Subseasonal to Seasonal (S2S) prediction project database. Bull Amer Meteor Soc 98:163–173. https://doi.org/10.1175/BAMS-D-16-0017.1

Vitart F, Balsamo G, Bidlot JR, Lang S, Tsonevsky I, Richardson D, Balmaseda M (2019) Use of ERA5 reanlysis to initialise re-forecasts proves beneficial. ECMWF Tech Memo, 841.

Zampieri L, Goessling HF, Jung T (2018) Bright prospects for Arctic sea ice prediction on subseasonal time scales. Geophys Res Lett 45:9731–9738. https://doi.org/10.1029/2018GL079394